ACS OMEGA

Open Access

http://pubs.acs.org/journal/acsodf

Article

Evaluation of Plant-Based Silver Nanoparticles for Antioxidant Activity and Promising Wound-Healing Applications

Maria Qubtia, Shazia Akram Ghumman,* Sobia Noreen, Huma Hameed, Shazia Noureen, Rizwana Kausar, Ali Irfan,* Pervaiz Akhtar Shah, Hafsa Afzal, Misbah Hameed, Mohammad Raish, Maria Rana, Ajaz Ahmad, Katarzyna Kotwica-Mojzych, and Yousef A. Bin Jardan*

Cite This: *ACS Omega* 2024, 9, 12146−12157

Read Online

ACCESS | Metrics & More | Article Recommendations

ABSTRACT: The current research focuses on the green synthesis of silver nanoparticles (AgNPs) using a polar extract of taro corms and the evaluation of its antioxidant properties and wound-healing applications. Taro corm extract (100 mL) was treated with a 5 mM $AgNO_3$ solution (100 mL) at room temperature for the formation of AgNPs, and a color change was observed. The surface plasmon resonance (SPR) peaks in their UV−visible spectra appeared at a range of 438−445 nm. Fourier transform infrared, scanning electron microscopy, energy-dispersive X-ray, dynamic light scattering, and X-ray diffraction were used for the characterization of the taro corms extract-mediated AgNPs (TCE-AgNPs). The synthesized AgNPs were crystalline and spherical, with an average size of 244.9−272.2 nm with a polydispersity index of 0.530 and zeta potential of −18.8 mV, respectively. The antibacterial potential of TCE-AgNPs was tested, and the inhibition zones detected against *Cronobacter sakazakii*, *Pseudomonas aeruginosa*, *Listeria monocytogenes*, and *Enterococcus faecalis* were 28, 26, 18, and 13 mm, respectively. Furthermore, the antioxidant activity of TCE-AgNPs showed significant radical-scavenging activity compared to the standard used. Collagen content data collected from regenerated tissue and higher collagen content indicated rapid wound healing compared to others, which was seen in a group treated with TCE-AgNP film bandages.

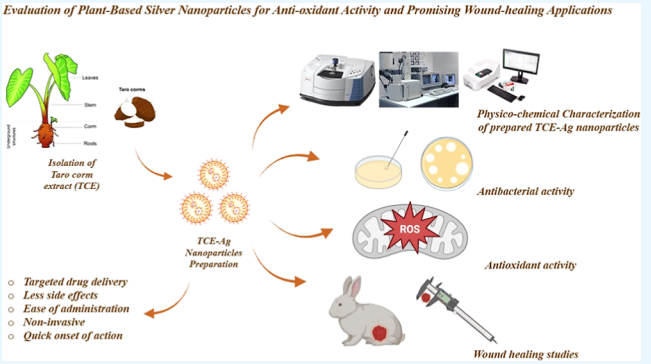

1. INTRODUCTION

Developments in nanotechnology have led to fascinating findings in the field of materials research.[1] The sectors of personal care products, ecological defense, nutrition, farming, and medical care can currently all benefit from the biological production of financially and ecologically advantageous silver nanoparticles (AgNPs).[2] Several parts of plants, such as roots, tubers, and fruit products, are typically employed in biological synthesis, also known as "green synthesis," which has numerous conventions.[3] Nanomaterials have the potential to be prepared using conventional chemical as well as physical approaches.[4] Nevertheless, biochemical methods have limitations like biotoxicity, which harms people and our surroundings, while traditional techniques require many resources.[5] Additionally, nanomaterials produced mechanically do not have the proper morphological measurement, content, clarity, size variation, or shape.[6] The enzymatic and antimicrobial sectors have developed and employed a variety of materials and metal-based oxide nanosystems. Among the many different forms of nanoparticles (NPs), AgNPs have drawn particular interest due to their distinctive physiochemical and photoelectric properties that render these as efficient fungicides and antibacterial, cancer-preventing, and enzymatic substances. AgNPs are increasingly valued because they can combat microorganisms that are resistant to antibiotics. Just two of the harmful species for which AgNPs exhibit substantial antimicrobial properties are *Staphylococcus aureus* and *Escherichia coli*.[7]

Incredibly, NPs made of "AgNPs" possess a wide range of applications in electronic devices, life sciences, and healthcare because of their limited plasmonic impact, great surface-to-volume proportion, and special physicochemical properties that make them useful.[8] Compared to other metal NPs, AgNPs have received much attention because of their frequent usage in several economically and biologically significant commodities.[9] The traditional methods of manufacturing, including physiological, thermal processing, hydrothermal, and biochem-

Received: December 29, 2023
Revised: February 13, 2024
Accepted: February 20, 2024
Published: March 1, 2024

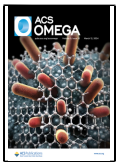

Figure 1. Schematic representation of TCE isolation and collection.

ical methods, are expensive and extremely unsafe and depend on dangerous materials. Therefore, the emphasis is on an environmentally friendly synthesis approach that makes use of biological substances for the efficient creation of NPs. The production of green NPs employing compounds that can be considered economically secure and recyclable as reduction and capping substances forms the foundation of the aforementioned beneficial procedure.[10]

The etiology of destructive diseases, including carcinoma, cerebrovascular problems, and diabetic complications, is linked to damage from oxidation, according to the findings. It has been demonstrated that radicals play a key role in preventing several ailments. The initiation or proliferation stages of a reactive response chain can be delayed or postponed by antioxidants as well, reducing reactive oxygen species (ROS)-mediated damage. AgNPs cause the formation of ROS, which deactivates the chain of respiration in cells. In doing so, they can also cause chromosomal harm to cancerous cells and stop the development of cells by causing death. One in six fatalities globally is thought to be related to cancer. Based on statistics, 10 million people will pass away in 2022 due to cancer-associated diseases. It is generally established that surroundings influence gene alterations that account for 90−95% of the total malignancies.[11] AgNPs have gained popularity relatively recently, particularly because of their potential antibacterial, antioxidant, and cancer-fighting abilities. Additionally, it is believed that the widespread usage of current pharmaceuticals is coming to an end because of the rise in bacterial organisms resistant to them brought on through overuse or improper ingestion. AgNPs could come into contact by binding to the microbial cell membrane's exterior and piercing it, making them a viable replacement for antibacterials.[12]

Taro is a significant tropical root crop cultivated specifically for its underground stems or starchy corms. It is recognized as a vital staple crop throughout the Pacific Islands, Asia, and Africa. A variety of carbohydrates, nutrients, and mineral substances, including iron, calcium, and potassium, that may go through fast oxidation are present in taro corms and are responsible for their increased utility as antioxidants.[13] Taro phytonutrients exhibit immunomodulatory, cancer-fighting, antimetastatic, antimutagenic, antihyperglycemic, and antihypercholesterolemic biological activities, as well as their antioxidant characteristics.[14] The use of taro, an intriguing replacement for regular food boasting less sugar than potatoes,

https://doi.org/10.1021/acsomega.3c10489
ACS Omega 2024, 9, 12146−12157

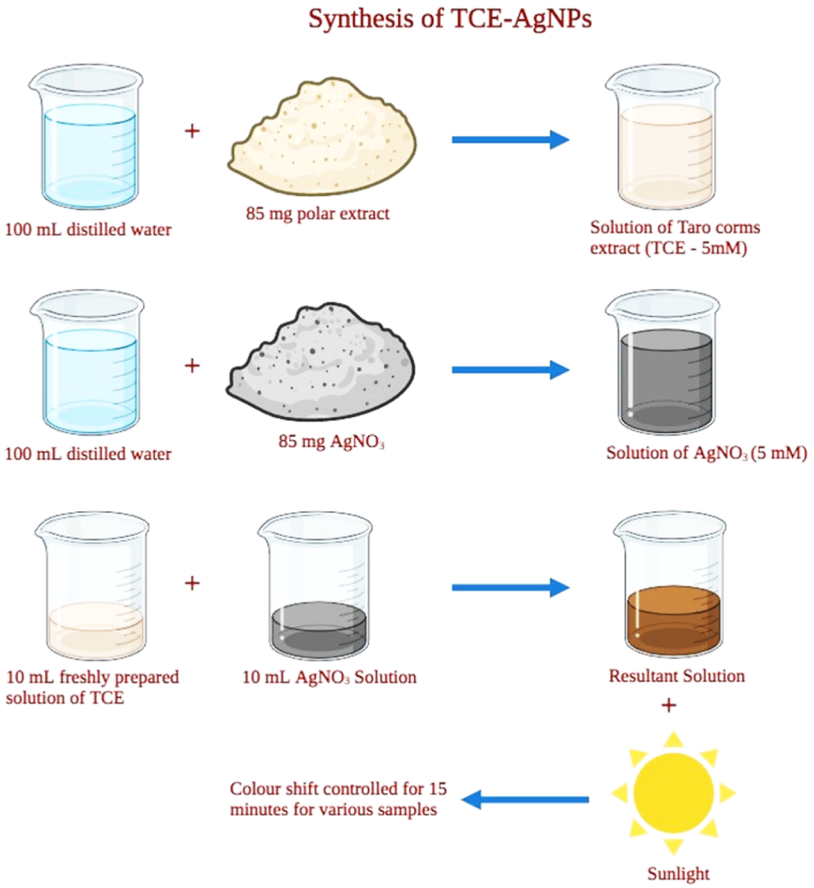

Figure 2. Preparation of the TCE-AgNPs.

might lower the rate and frequency of several illnesses, including specific malignancies.[15] Investigators have previously documented the effective production of PEG-based palladium taro corm NPs and ZnO/Ag nanocomposites from the extract of taro leaves.[16] In terms of amount and variety, the dietary component of taro is an abundant supply of antioxidants, namely, phenolic chemical substances.[17] The main objective of this research was to use the polar extract of taro corms to optimize the extraction process, and we further studied the antioxidant and antibacterial activity. The wound-healing ability and collagen content of the taro corm extract (TCE) films were estimated for the first time.

2. MATERIALS AND METHODOLOGY

2.1. Materials. Taro corms used for mucilage extraction were purchased from a local market. $AgNO_3$ was procured from Merck in Germany. 2,2-Diphenylpicrylhydrazyl (DPPH) was obtained from Merck-Germany. All reagents and solvents were of analytical grade, and deionized water was used for the extraction of TCE and the preparation of all solutions.

2.2. Isolation of TCE. Taro corms were carefully and thoroughly cleaned by using distilled water. The corm's outer surface was removed; small pieces of a particular size of corms were dried for 15 days at room temperature. The corms were crushed by a grinder after drying and then passed through a sieve. 2.5 g of fine-dried corm powder was thoroughly mixed in 50 mL of distilled water in 100 mL and was stirred at room temperature for 5 h on a hot plate. The solution was filtered via Whatman paper, and a separating funnel was used to wash the filtrate with *n*-hexane. Two layers formed after washing with *n*-hexane, i.e., polar and nonpolar. The nonpolar layer was discarded, while the polar layer was poured into a Petri dish and dried for 24 h at 45 °C in a drying oven. The polar sample was removed from the Petri dish after drying and stored in a freezer.[18] A schematic representation of the isolation and collection of TCEs is shown in Figure 1.

2.3. Synthesis of TCE-AgNPs. The solution of TCE (5−5 mM) was freshly prepared in 100 mL of distilled water by dissolving 85 mg of polar extract and $AgNO_3$ (5 mM) by dissolving 85 mg of $AgNO_3$ in 100 mL of distilled water. Then 10 mL of freshly prepared TCE solution was drawn into a 50 mL beaker and added to 10 mL of the $AgNO_3$ solution. The response combination was irradiated with sunlight, and the color shift was controlled for up to 15 min for various samples, as explained in Figure 2.[19]

2.4. Characterization of the Synthesized TCE-AgNPs. *2.4.1. UV−Visible Analysis.* UV−vis analysis was performed for the characterization of the synthesized TCE-mediated AgNPs (TCE-AgNPs). A specimen (1.0 mL) of the reactant mixture was obtained at specific time intervals (1, 2, 5, 10, 15, and 20 min) and investigated in a range of 200−800 nm using a UV−vis spectrophotometer (UV-1700 PharmaSpec, Shimadzu).[20]

2.4.2. Fourier Transform Infrared Spectroscopy and Thermogravimetric Analysis. Fourier transform infrared (FTIR) spectroscopy was carried out to check various components of the sample and synthesize AgNPs. Infrared spectra were acquired of TCE and TCE-AgNPs using the method of KBr pellets with a range of 500−4000 cm^{-1} via the IR prestige-21 Shimadzu Germany.

https://doi.org/10.1021/acsomega.3c10489
ACS Omega 2024, 9, 12146−12157

2.4.3. X-ray Diffraction. X-ray diffraction (XRD) is a nondestructive process for identifying the NP's crystal structure. Each crystalline solid has a distinctive structure of the atom and a distinctive pattern of XRD. These patterns are used to define the fingerprints of the crystal configuration. The powdered sample was put on a sample holder and then illuminated with set wavelength X-rays, and the reflected radiation intensity was measured. Powder XRD (PXRD) analysis on a diffractometer (JEOL X-ray diffractometer system JDX-3532) with monochromatic X-rays was performed (over a range of 5−70°, 2Ø).[21]

2.4.4. Energy-Dispersive X-ray and Scanning Electron Microscopy. Energy-dispersive X-ray (EDX) spectroscopy and scanning electron microscopy (SEM) can potentially be employed together to analyze the chemical composition of AgNPs and study their form. The sample slide was arranged and examined at various resolutions using the JEOL JSM-IT100 at a voltage of 5 kV.[22]

2.4.5. Particle Size Distribution. Dynamic light scattering (DLS) (Nano ZS Zetasizer system, Malvern Instruments) using a He−Ne laser beam (633 nm) and a temperature of 25 °C has been employed to determine the range of particle sizes in the resulting solution. This analysis provides the polydispersity index (PDI) that demonstrates the particle size distribution. Before DLS measurements, various amounts of TCE-AgNPs were diluted, and a 0.22 μm syringe was employed to filter them.[23]

2.4.6. Zeta Potential Measurements. The zeta potential quantifies the electrostatic repulsion between an NP's surface and the surrounding fluid, which contains ions with the opposite charge. The NPs' zeta potential is less than or equal to −28 mV, indicating that they are agglomerated. A zeta sizer (Malvern Zetasizer ZS-90, Malvern Instruments Ltd., U.K.) was used for DLS analysis to quantify particle size and to evaluate the zeta potential of the TCE-AgNPs.[24]

2.5. Antibacterial Assay. *2.5.1. Bacterial Strains.* To direct investigations, discoveries, and the creation of novel medicines, the World Health Organization established a worldwide target set of microorganisms tolerant to antibiotics in 2017 including *Cronobacter sakazakii*, *Pseudomonas aeruginosa*, *Shigella* spp., *Listeria monocytogenes*, *Enterococcus faecalis*, and so on. It implies that such microbes require innovative antibiotics immediately.[25] So for antibacterial activity testing, the bacteria *C. sakazakii* (ATCC#29544), *P. aeruginosa* (ATCC#10145), *L. monocytogenes* (ATCC#13932), and *E. faecalis* (ATCC#14506) have been selected. For bacterial cultivation, dissolving 4 g of nutrient broth in 100 mL of distilled water made the nutrient medium for bacterial inoculant growth, adjusting the pH to 7.0 and autoclaving the solution, which was then poured (25 mL) into the Petri plates under the laminar flow cabinet. First of all, media were sterilized and poured into Petri plates inside the laminar flow cabinet, and then the Petri plates were labeled; in one Petri plate, *C. sakazakii* (ATCC#29544) was inoculated. A similar method was carried out for *P. aeruginosa* (ATCC#10145), *L. monocytogenes* (ATCC#13932), and *E. faecalis* (ATCC#14506). Then all Petri plates were incubated for 24 h at 37 °C. The turbidity of the bacterial cultures was checked. Now the bacterial strains were fully active and ready to grow on Petri plates.[26]

2.5.1.1. Experimental Procedure. For media preparation, 4.3 g of agar was dissolved in 100 mL of distilled water. The agar solution and Petri plates were then autoclaved for 20 min at 121 °C. After sterilization, each Petri platform was filled with 25 mL of agar solution to enable it to solidify over 20 min. After that, the stick plate method fulfilled the required bacterial strain in each Petri dish. Five wells were created by the cork borer after sticking and marked alphabetically. The entire procedure was then carried out in a well with 30 μL of distilled water as the negative control, 30 μL of erythromycin (1 mg/mL) as the positive control, 30 μL of AgNPs, 30 μL of plant extract, and 30 μL of $AgNO_3$ solution and subsequently incubated in a laminar flow and sterile laboratory conditions at 37 °C for 24 h.

2.6. Antioxidant Activity. *2.6.1. Ferric Reducing Antioxidant Power Assay.* The ferric reducing antioxidant power (FRAP) assay was used to evaluate the antioxidant activity. Distilled water was used to dilute the taro corm polar extract and TCE-AgNPs to values ranging from 10 to 50 mg/L. Ascorbic acid solution is used as a benchmark in FRAP assays. Concentrations of 10, 20, 30, 40, and 50 mg/L were used as the reference standard solutions. To make phosphate buffer saline (pH 6.6), 8 g of sodium chloride, 0.2 g of potassium chloride, 1.44 g of disodium hydrogen phosphate, and 0.24 g of potassium dihydrogen phosphate were dissolved in 500 mL of deionized water, then HCL was added until the pH reached 6.6, and it was finally diluted to 1000 mL with more deionized water.[27,28] To the samples and controls were added 2.5 mL of phosphate buffer (pH 6.6) and 2.5 mL of 1% $K_3Fe(CN)_6$. The mixture was shaken in a vortex for 5 min before being incubated at 50 °C for 20 min. Following incubation, 2.5 mL of 10% TCA was added to the mixture, and then the contents were centrifuged (3000 rpm for 10 min). After centrifugation, the supernatant was collected and diluted with deionized water to a concentration of 2.5 mL. A colorful solution was obtained by adding 0.51 mL of 0.1% ferric chloride to the mixture. A UV−visible spectrophotometer set to 711 nm was used to analyze the samples and reference standard solutions.[29]

2.6.2. DPPH Radical-Scavenging Capacity Assay. After a few changes were made to the procedure, the DPPH test was performed. A methanol solution of DPPH (4 mg/100 mL) was combined with aliquots of each TCE-AgNP (1, 2, 3, 4, and 5 mL) to a final volume of 6 mL. The absorbance of the solutions was then measured at 517 nm after 15 min of incubation at room temperature in the dark. A DPPH blank was made and analyzed (5.4 mL of methanol and 600 mL of DPPH solution).[30] The percentage of inhibition was estimated by observing the absorbance drop at each concentration and then plugging those values into the following formula

$$\% \text{ inhibition} = \frac{(\text{A of control} - \text{A of sample})}{\text{A of control}} \times 100$$

2.7. Designing of a Wound-Dressing Patch. The prepared TCE-embedded AgNPs were converted to a dressing patch. A mixture of TCE-AgNPs was spread into the Petri dish and covered with aluminum foil to make a film-type patch by putting it in an oven at 50 °C for hours. After film formation, films were stored in an airtight container for wound-healing studies.[31]

2.7.1. Wound-Healing Experiment. First of all, this study protocol was approved by the Ethical Committee of the University of Sargodha (UOS), Sargodha, under ref no. 20−2023/PREC and by the animal handling and care guidelines mentioned by the National Institute of Health (NIH). 15 healthy rabbits (2 ± 0.3 kg, 3−4 months old) were selected and divided into three equal groups: positive control (wound

https://doi.org/10.1021/acsomega.3c10489
ACS Omega 2024, 9, 12146−12157

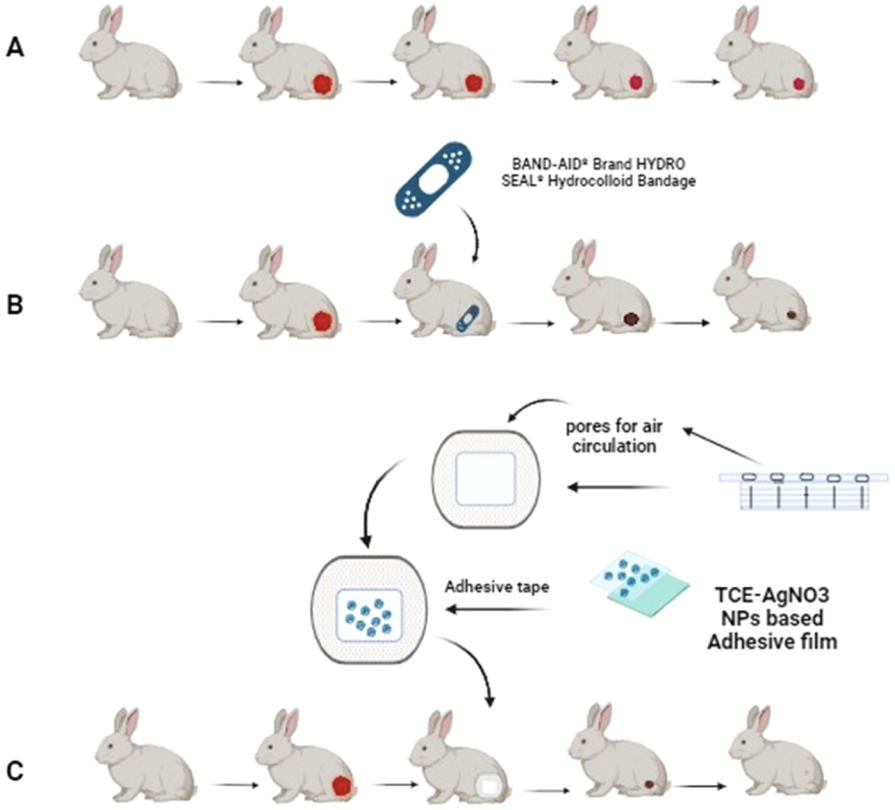

Figure 3. Complete illustration of the wound-healing experiment; three equal groups: (A) positive control (wound excision done), (B) standard (wound excision with marketed available bandage), and (C) tested one (wound excision plus prepared TCE-AgNP film bandage).

excision done), standard (wound excision with marketed available bandage), and tested one (wound excision plus prepared TCE-AgNP film bandage). All of the animals were supplied with standard food and water throughout the study. Local anesthesia was given to all three groups. Hair was removed from the leg of the rabbit, and with the help of biopsy forceps, a circular wound of 1 cm in diameter was created. The wound was left open in the positive control group of rabbits and was left untreated. A market-available bandage (BAND-AID Brand HYDRO SEAL Hydrocolloid Bandage) was applied to the standard group with the wound. The test group was treated with prepared TCE-AgNP films with adhesive tape. After this, all the groups were examined for 2 weeks, and the wounded-to-recovered area was calculated at different intervals by tracing it on tracing paper. All three groups were statistically compared.[31] An illustration of the whole procedure is shown in Figure 3.

2.7.2. Estimation of Collagen. Regenerated tissue-linked collagen content was measured in all three groups using a reported method.[32] For this purpose, the scratched wound was collected from the regenerated tissue. After this, the scratched wound was chopped, washed with 0.5 M sodium acetate, and suspended in 0.5 M acetic acid (10% w/v). Then the mixture was stirred for 36 h and centrifuged at 5000 rpm for 1 h and 30 min. After centrifugation, sodium chloride (10% w/v) was added to precipitate collagen, which was then separated via filtration. The amount of collagen was calculated using the following equation

$$\text{Amount of collagen}\left(\frac{\text{mg}}{\text{kg}}\right) = \text{Total weight of filter paper plus filtrate after filtration} - \text{weight of filter paper before filtration}$$

2.8. Statistical Analysis. All the collected results were expressed as the mean ± standard deviation after analysis by one-way ANOVA. A p-value < 0.05 was considered statistically significant.

3. RESULTS AND DISCUSSION

3.1. Green Synthesis of AgNPs and TCE-AgNPs. When the $AgNO_3$ solution was exposed to sunlight, hydrated electrons were produced in the system. It is possible to use these electrons to reduce monovalent silver cations to zerovalent silver atoms, which generally have a nanometer range of size. In the current study, we used a polar extract of taro corms to perform the green synthesis of AgNPs as a green-reducing agent under sunlight. TCE-AgNP synthesis was performed using an $AgNO_3$ solution concentration of 5 mM. Then the reactant was mixed, and Ag^+ reacted with the polar extract of taro corms in $AgNO_3$ to give the TCE-AgNP complex.[33]

3.2. Characterization of the Synthesized AgNPs: Analysis through UV−Visible Spectroscopy. Using UV−visible spectrophotometry, the synthesis of AgNPs with a polar extract of taro corms was investigated. The sample stored in the dark showed no UV spectrum. The color of the solution differs with time, by reducing Ag^+ to Ag^0 when exposed to sunlight. The combined oscillation of conducting electrons in

https://doi.org/10.1021/acsomega.3c10489
ACS Omega 2024, 9, 12146−12157

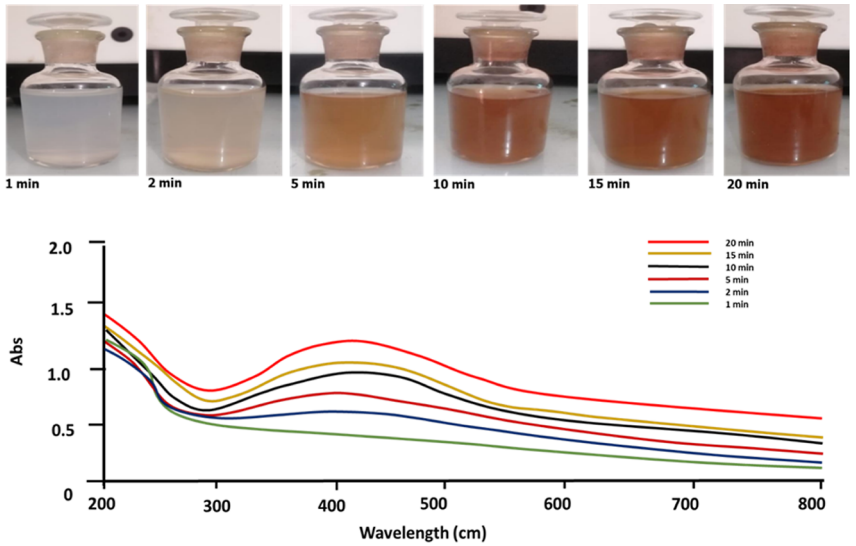

Figure 4. (A) TCE-Ag mixture presenting color change with time. (B) UV−vis spectrum data of synthesized TCE-AgNPs.

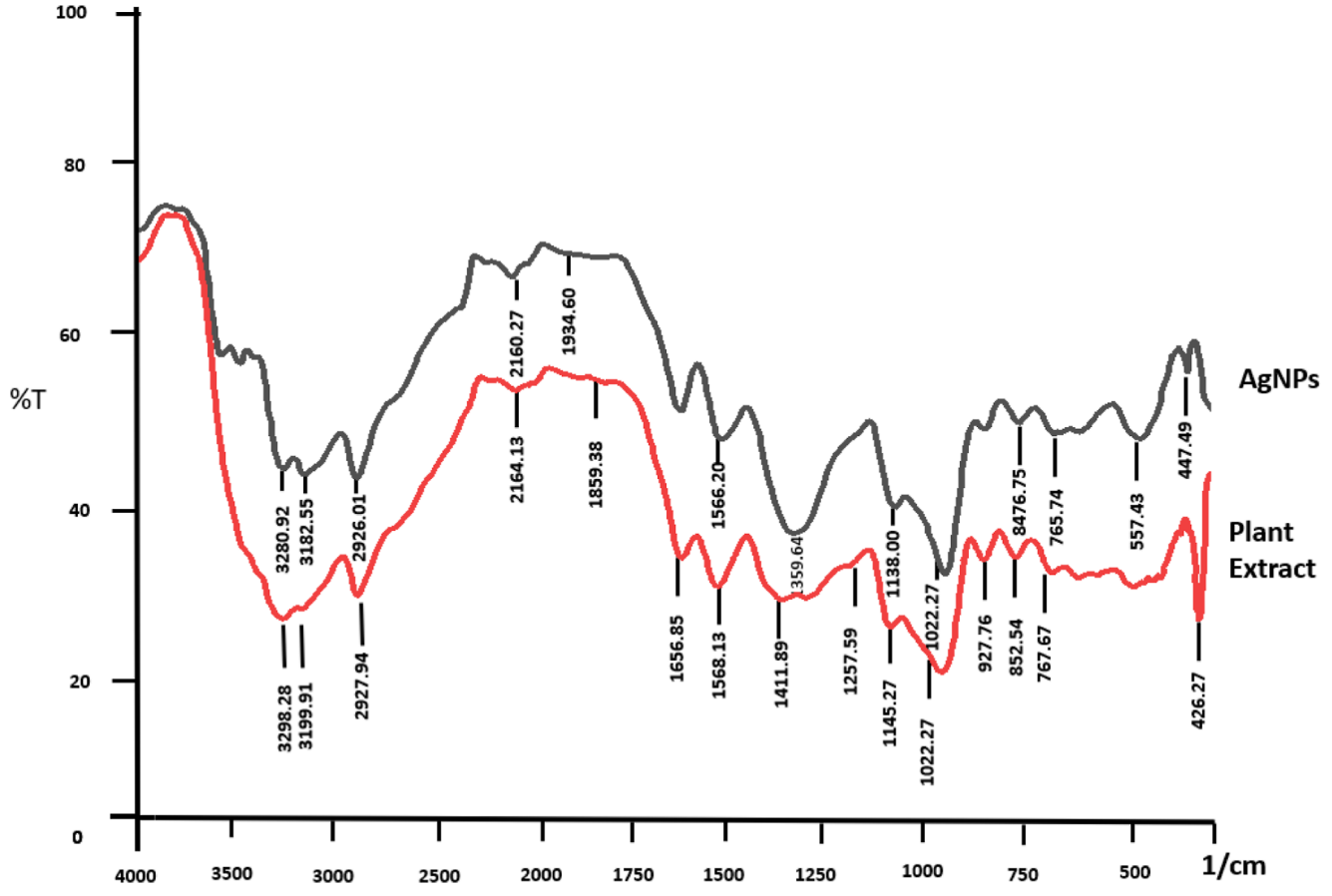

Figure 5. Spectra of the polar extract of the taro corms polar extract and TCE-AgNPs.

TCE-AgNPs has contributed to the strong absorption of the surface plasmon resonance (SPR) phenomenon within the visible range. The SPR transition relay showed changes in color from yellowish-brown to reddish-brown in the dimension and reaction time of TCE-AgNPs.[34] The typical SPR peaks in their UV−visible spectra of TCE-AgNPs appeared at a range of 438−445 nm, showing the synthesis of TCE-AgNPs at corresponding reaction times: 1, 2, 5, 10, 15, and 20 min. As the size of TCE-AgNPs increases, the wavelength of the absorbed light (red shift) increases over time.[35] Absorption intensity also increased with time, from 1 to 20 min, suggesting a steady decrease in Ag^+ ions by taro corms, as shown in Figure 4.

3.3. FTIR Spectroscopy. FTIR spectra of the plant extract and TCE-AgNPs are shown in Figure 5. These spectra help identify the metabolites responsible for Ag ion reduction. Distinctive peaks between 3299 and 3182 cm^{-1} appear both in plant extract and TCE-AgNPs and confirm the presence of the

https://doi.org/10.1021/acsomega.3c10489
ACS Omega 2024, 9, 12146−12157

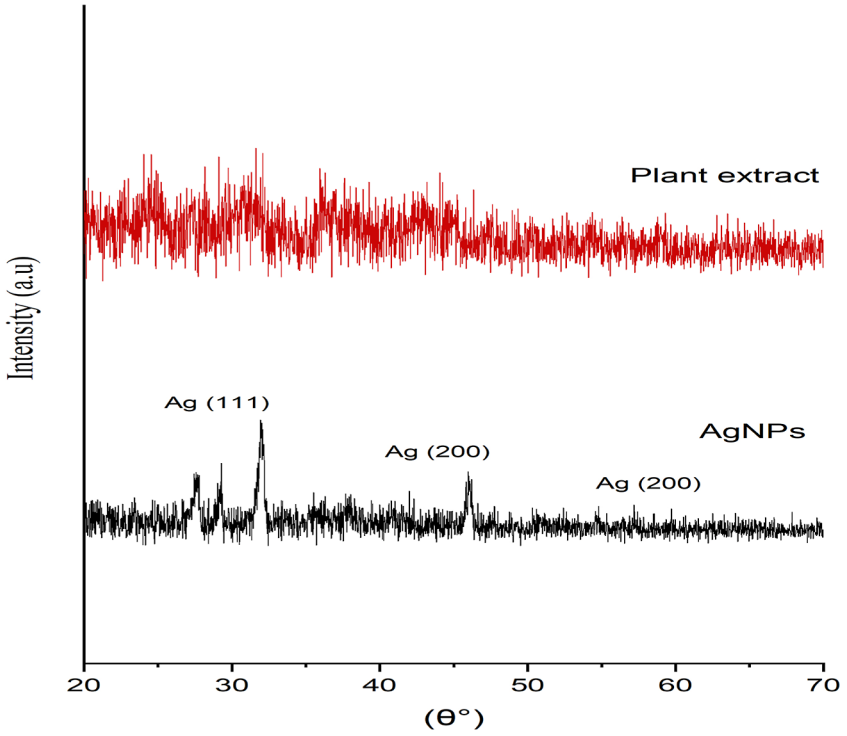

Figure 6. PXRD spectra of TCE and TCE-AgNPs.

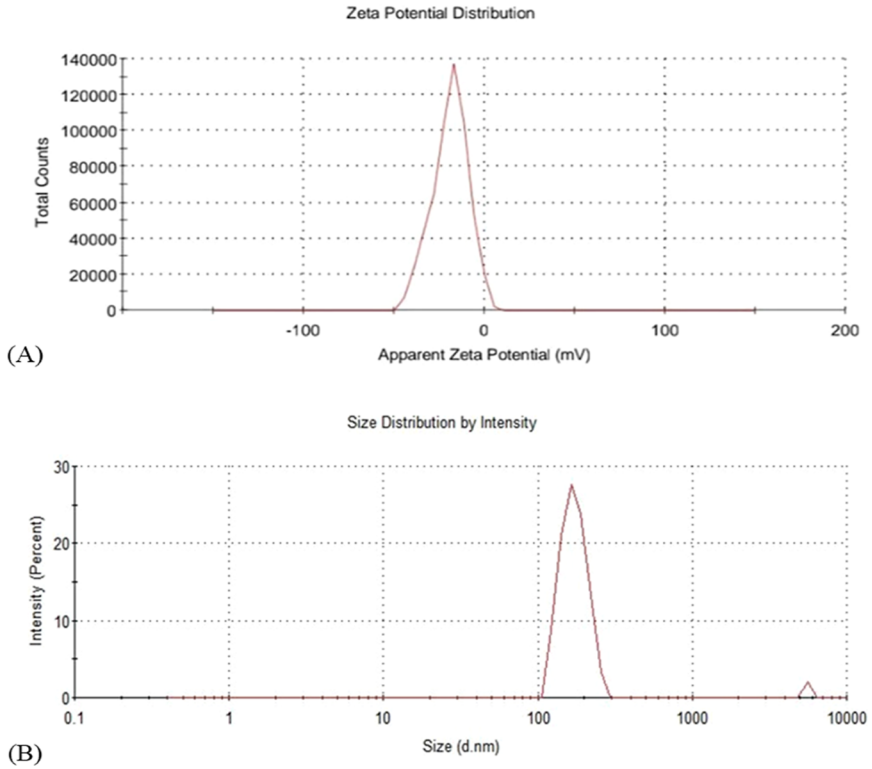

Figure 7. (A) Size distribution pattern of TCE-AgNPs. (B) Zeta potential pattern of TCE-AgNPs.

OH group of alcohols and phenols.[36] The absorption bands at 2927.96 and 2926.01 cm^{-1} correspond to alkanes. The peaks 2164.13 and 2160.27 cm^{-1} indicate the presence of alkynes, N−C, and N═C groups in the R−N═C═S structure.[37] The absorption peaks at 1934.60 cm^{-1} in NPs and 1859.38 cm^{-1} in plant extract point toward the presence of C−H bending of aromatic compounds.[38] A band at 1656.85 cm^{-1} in plant extract corresponds to amide I and the peaks at 1568.13 and 1566.20 cm^{-1} are possibly due to amide II in proteins.[39] The band at 1411.89 cm^{-1} in the plant extract specifies the S═O (sulfate ester) group. The bands at 1145.27 and 1138.00 cm^{-1} confirmed the carboxylic acid group in both. Another band at

https://doi.org/10.1021/acsomega.3c10489
ACS Omega 2024, 9, 12146−12157

1022 cm^{-1} represents the CH_3 bond vibrations.[40] Proteins can bind to metals in NPs by using their free carboxylate groups and stabilize the product.[41] A comparison of the FTIR spectra of both the taro extract and TCE-AgNPs indicated a minor shift in the position of a few of the absorption peaks. These changes confirmed the involvement of plant extract metabolites in AgNP formation. OH and CO groups present in plant extract play a key role in the reduction and stabilization of NPs.[42]

3.4. Powder X-Ray Diffraction. The PXRD study verified the crystal phase of the TCE-AgNPs, as shown in Figure 6, as numeral of Bragg's reflections with 2θ values of −38.2, 44.3, and 67.6° arrays of the framework were detected that indexed to (111), (200), and (220) indicated facets of Ag^0. The XRD results verified the presence of the crystalline nature of synthesized AgNPs.[43]

3.5. Zeta Potential and Particle Size Measurements. DLS is an efficient and statistically valid method for determining the particle size distribution of nanoscale materials dispersed in solution or colloidal suspensions. As a function of intensity, the size distributions of the synthesized AgNPs are shown in Figure 7. Moreover, the surface charges of the synthesized AgNPs were disclosed by measuring their zeta potential, which was found to be −18.8 mV (Figure 7A), indicating the increased stability of the particles.[44] The significant negative potential may be attributable to the polyphenolic capping components of the extract. This finding suggests that the existence of repulsive forces can prevent particles from aggregating and agglomerating, leading to long-term stability. Based on laser diffraction analysis, it was observed that the collected particles were a polydisperse mixture (Figure 7B). The average particle size was calculated to be 244.9−272.2 nm with a PDI of 0.530.

3.6. SEM and EDX Analyses. A scanning electron microscope is used to determine the surface morphology of the synthesized NPs in terms of shape, size, and size distributions.[44] Synthesized AgNPs have been observed in various shapes, including spherical, oval, triangular, cubic, and pebble-like. They may appear in a single or aggregate form. Morphological variations were caused by applied conditions and the concentration of feed.[45] Micrographs shown in Figure 8 reveal that the synthesized TCE-AgNPs were crystalline,

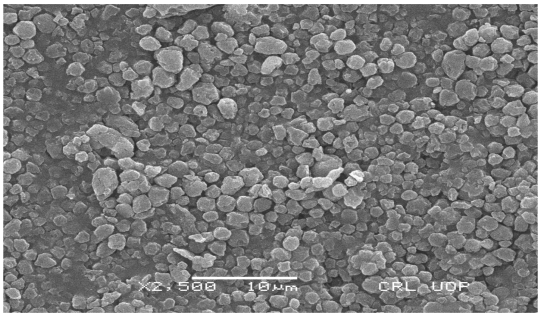

Figure 8. SEM images of TCE-AgNPs.

homogeneously dispersed, and almost spherical. Crystallization may be due to polyphenolic compounds in the plant extract, and these polar groups bind with Ag. A similar morphology was observed for various plant-based AgNPs.[46,47] In the EDX studies presented in Figure 9, silver showed a weight percentage of 64.19 and an atomic percentage of 18.56. The

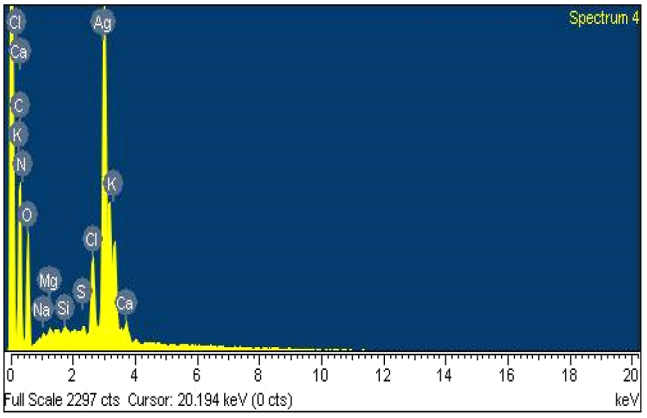

Figure 9. EDX spectrum showing the presence of silver in TCE-AgNPs.

EDX spectrum specified peaks corresponding to Ca, O, Cl, C, K, N, Mg, Na, Si, and S. Distinctive peaks between 2.7 and 3.4 keV designated silver metal. The other signals could be due to phytoconstituents that coat the AgNPs' surface produced with TCE.[48]

3.7. Antibacterial Activity. Silver itself and its various modalities have been found to affect antimicrobial agents.[49] The exceptional antibacterial activity of AgNPs against various infectious and pathogenic bacteria has attracted the attention of researchers as well as industries to formulate a wide variety of NPs using various types of materials, including biodegradable and renewable biopolymers.[50] TCE-AgNPs' antibacterial activity was studied against various pathogenic bacteria, such as *C. sakazakii* (ATCC#29544), *P. aeruginosa* (ATCC#10145), *L. monocytogenes*(ATCC#13932), and *E. faecalis* (ATCC#14506), using the well diffusion method. Synthesized AgNPs suppressed the growth of both Gram-negative and Gram-positive bacterial strains comparable to the negative control (A), as shown on the Petri dishes. Figure 10 shows the inhibition zones (mm) with AgNP solutions around each well. The inhibition zones detected against *C. sakazakii*, *P. aeruginosa*, *L. monocytogenes*, and *E. faecalis* were 28, 26, 18, and 13 mm, respectively. These results confirmed that the synthesized AgNPs have a significantly high growth-suppression ability against the selected strains of bacteria.

3.8. Antioxidant Activities of TCE-AgNPs. *3.8.1. FRAP Assay.* The reducing ability reflects the antioxidant potential of a formulation by fixing the intermediates of oxidation reactions.[51,52] The FRAP assay is used for screening the antioxidant abilities and comparing the efficiencies of various compounds. During this assay, a colorless Fe^{3+} complex reacts with a potential antioxidant and reduces to an intense blue Fe^{2+} complex.[52] It is a facile, suitable, reproducible, and widely accepted method to assess antioxidant efficiency.[53] The results of various concentrations of formulations (10−50 ppm) showed % RSA ranging from 31.15 to 37.38% as presented in Figure 11A. Generally, the antioxidant potential of AgNPs depends on the chemical moieties present in the extract. If the plant extract is rich in flavonoids and phenolic compounds, the NPs showed high scavenging activity.[54] The O−H functional group mediated the antioxidant effect of these metabolites.[55] The free O−H group on the aromatic ring is responsible for the antioxidant properties. The hydrogen of O−H on the aromatic ring was donated to the free radical, resulting in the stability of free radical species.[56] These results confirmed the

https://doi.org/10.1021/acsomega.3c10489
ACS Omega 2024, 9, 12146−12157

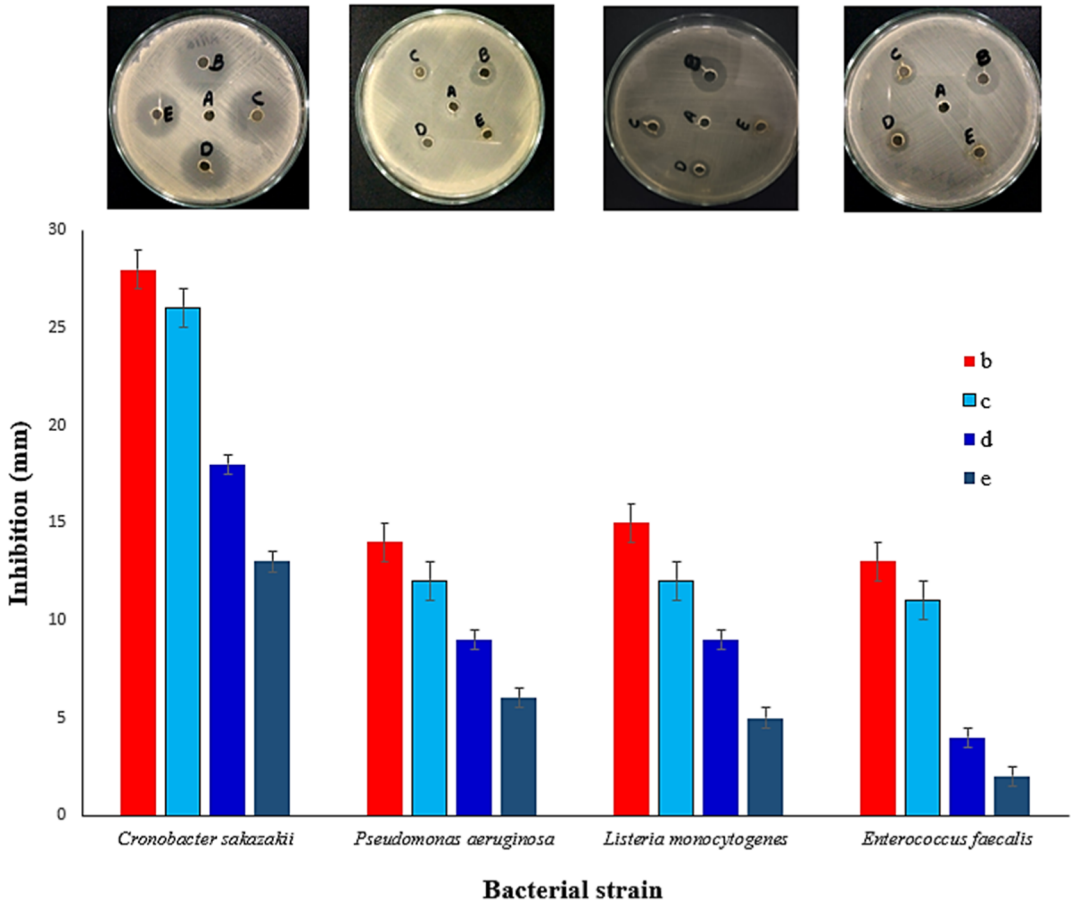

Figure 10. Inhibition zone and antibacterial activity against 4 mentioned strains; (A) negative control, (B) positive control, (C) TCE-AgNPs, (D) plant extract, and (E) $AgNO_3$.

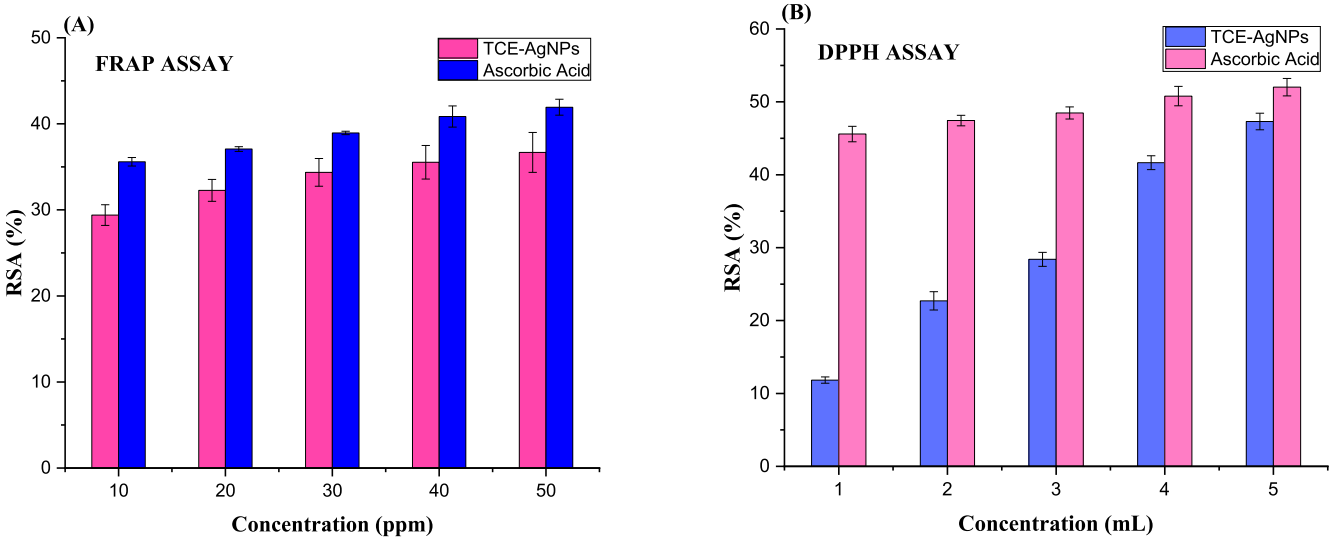

Figure 11. Antioxidant activities of TCE-AgNPs; (A) FRAP assay and (B) DPPH assay.

antioxidant abilities of TCE-AgNPs and agree with previously studied plant-based AgNPs.[19]

3.8.2. DPPH Radical-Scavenging Capacity Assay. The DPPH free radical shows a characteristic absorption peak at 517 nm. The decline in absorbance value indicates the radical-scavenging ability of the formulation.[53] The free radical-scavenging ability of TCE-AgNPs was determined by the DPPH assay. The 50% inhibitory or radical-scavenging concentration was used to estimate the DPPH radical-scavenging activity. The results are shown in Figure 11B, where TCE-AgNPs showed significant radical-scavenging activity as compared to the standard used. The scavenging activity increased with an increasing concentration.

3.9. Analysis of Wound-Healing Experiment. All three groups were analyzed for 2 weeks for the healing of excision wounds that were created on the leg of each rabbit. After the

https://doi.org/10.1021/acsomega.3c10489
ACS Omega 2024, 9, 12146−12157

Table 1. Reduction in the Wound Diameter (mm) Indicating Wound Healing in All Three Groups at Different Intervals

	1st	3rd	5th	8th	11th	14th
control group	6.18 ± 0.08	5.98 ± 0.06	4.78 ± 0.03	3.48 ± 0.08	2.46 ± 0.04	1.46 ± 0.04
standard group	6.15 ± 0.12	5.83 ± 0.04	3.78 ± 0.09	1.86 ± 0.02	0.98 ± 0.06	0.14 ± 0.02
treated group	6.21 ± 0.09	5.64 ± 0.03	3.12 ± 0.08	1.11 ± 0.04	0.08 ± 0.02	0.00

results were collected, the average was taken for each group. Reduction in wound area closure was taken as a healing parameter. The control group showed a delay in wound closure compared to both the standard and treated groups. Even the treated group showed rapid recovery in comparison with that of the standard group. Overall, all the results collected from the three groups were comparable and are summarized in Table 1.

Reduction in wound diameter was a clear indication of wound healing, but collagen content has an important role in the mechanism of wound healing, and it was also checked in all three groups. Collagen content data collected from regenerated tissue for all three groups are mentioned in Figure 12. Higher collagen content was an indication of rapid healing in a group as compared to others, which was seen in a group treated with TCE-AgNP film bandages.

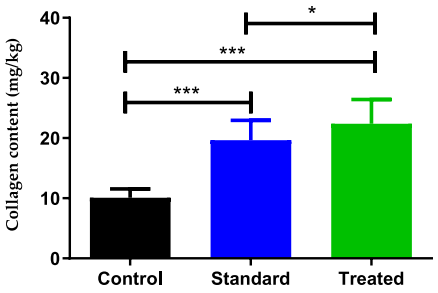

Figure 12. Estimation of collagen content in three equal groups: control (wound excision done), standard (wound excision with marketed available bandage), and tested one (wound excision plus prepared TCE-AgNPs film bandage). Note: Statistical significance from control group and is shown by $*p < 0.05$.

4. CONCLUSIONS

In this study, our team designed an ecofriendly, cost-effective TCE-AgNPs-based film bandage using biodegradable and nontoxic TCE with good antibacterial and antioxidant activities. In vitro characterization and in vivo wound-healing activities were performed to check the pharmacological activity of TCE-AgNPs. TCE-AgNP films provide extra stability and a better storage medium for AgNPs for prolonged periods and facilitate patient compliance because of the ease of administration. AgNPs embedded with TCE films can be exploited for commercial purposes as a potential antimicrobial and wound-healing bandage.

AUTHOR INFORMATION

Corresponding Authors

Shazia Akram Ghumman − *College of Pharmacy, University of Sargodha, Sargodha 40100, Pakistan*; Email: shazia.akram@uos.edu.pk

Ali Irfan − *Department of Chemistry, Government College University Faisalabad, Faisalabad 38000, Pakistan*; orcid.org/0000-0002-8977-3303; Email: raialiirfan@gmail.com

Yousef A. Bin Jardan − *Department of Pharmaceutics, College of Pharmacy, King Saud University, Riyadh 11451, Saudi Arabia*; Email: ybinjardan@ksu.edu.sa

Authors

Maria Qubtia − *College of Pharmacy, University of Sargodha, Sargodha 40100, Pakistan*

Sobia Noreen − *Institute of Chemistry, University of Sargodha, Sargodha 40100, Pakistan*; orcid.org/0000-0002-0815-2223

Huma Hameed − *Faculty of Pharmaceutical Sciences, University of Central Punjab, Lahore 54000, Pakistan*

Shazia Noureen − *Institute of Chemistry, University of Sargodha, Sargodha 40100, Pakistan*

Rizwana Kausar − *ILM College of Pharmaceutical Sciences, Sargodha 40100, Pakistan*

Pervaiz Akhtar Shah − *University College of Pharmacy, University of the Punjab, Lahore 54000, Pakistan*

Hafsa Afzal − *Institute of Pharmacy, Faculty of Pharmaceutical and Allied Health Sciences, Lahore College for Women University, Lahore 54000, Pakistan*

Misbah Hameed − *Institute of Pharmacy, Faculty of Pharmaceutical and Allied Health Sciences, Lahore College for Women University, Lahore 54000, Pakistan*

Mohammad Raish − *Department of Pharmaceutics, College of Pharmacy, King Saud University, Riyadh 11451, Saudi Arabia*

Maria Rana − *Riphah Institute of Pharmaceutical Sciences, Riphah International University Lahore Campus, Lahore 54000, Pakistan*

Ajaz Ahmad − *Department of Clinical Pharmacy, College of Pharmacy, King Saud University, Riyadh 11451, Saudi Arabia*

Katarzyna Kotwica-Mojzych − *Chair of Fundamental Sciences, Department of Histology, Embryology and Cytophysiology, Collegium Medicum, 20-080 Lublin, Poland*

Complete contact information is available at: https://pubs.acs.org/10.1021/acsomega.3c10489

Author Contributions

M.Q.: Methodology, Formal Analysis, Writing—Original Draft, Data Curation, and Investigation; **S.A.G.:** Conceptualization, Supervision, Project Administration, Writing—Review and Editing, and Investigation; **Sobia Noreen:** Conceptualization, Co-Supervision, Validation, and Writing—Review and Editing; **H.H.:** Conceptualization, Co-Supervision, Visualization, and Writing—Review and Editing; **Shazia Noureen:** Writing—Original Draft, Data Curation, and Validation; **R.K.:** Formal Analysis and Visualization; **A.I.:** Formal Analysis, Funding Acquisition, Visualization, and Writing—Review and Editing; **P.A.S.:** Data Curation, Resources, and Writing—Review and Editing; **H.A.:** Data Curation; Visualization, and Writing—Review and Editing; **M.H.:** Visualization, Resources, and Review and Editing; **Mohammad Raish:** Formal Analysis, Funding Acquisition, Data Curation, and Writing—Review and Editing; **Maria Rana:** Investigation, Visualization, and

https://doi.org/10.1021/acsomega.3c10489
ACS Omega 2024, 9, 12146−12157

Writing—Review and Editing; **A.A.:** Formal Analysis, Validation, and Data Curation; **K.K.-M.:** Validation, Formal Analysis, Writing—Review and Editing, and Data Curation; **Y.A.B.J.:** Funding Acquisition, Project Administration, Methodology, Resources, and Writing—Review and Editing.

Funding

The project grant RSP2024R457 was received from King Saud University, Riyadh, Saudi Arabia to support this research.

Notes

The authors declare no competing financial interest.
This study protocol was approved by the Ethical Committee of the University of Sargodha (UOS), Sargodha under ref no 20−2023/PREC and by the animal handling and care guidelines mentioned by the National Institute of Health (NIH).

■ ACKNOWLEDGMENTS

The authors would like to extend their sincere appreciation to the Researchers Supporting Project , King Saud University, Riyadh, Saudi Arabia for funding this work through the project number (RSP2024R457).

■ REFERENCES

(1) Hulla, J.; Sahu, S.; Hayes, A. Nanotechnology: History and future. *Hum. Exp. Toxicol.* **2015**, *34* (12), 1318−1321.
(2) Rehman, I.; Gondal, H. Y.; Zamir, R.; Al-Hussain, S. A.; Batool, F.; Irfan, A.; Noreen, S.; Roheen, T.; Nisar, M.; Zaki, M. E. A. Green Synthesis: The Antibacterial and Photocatalytic Potential of Silver Nanoparticles Using Extract of Teucrium stocksianum. *Nanomaterials* **2023**, *13* (8), 1343.
(3) Baran, A.; Keskin, C.; Baran, M. F.; Huseynova, I.; Khalilov, R.; Eftekhari, A.; Irtegun-Kandemir, S.; Kavak, D. E. Ecofriendly synthesis of silver nanoparticles using ananas comosus fruit peels: anticancer and antimicrobial activities. *Bioinorg. Chem. Appl.* **2021**, *2021*, 1−8.
(4) Zulfiqar, H.; Amjad, M. S.; Mehmood, A.; Mustafa, G.; Binish, Z.; Khan, S.; Arshad, H.; Proćków, J.; Pérez de la Lastra, J. M. Antibacterial, antioxidant, and phytotoxic potential of Phytosynthesized silver nanoparticles using Elaeagnus umbellata fruit extract. *Molecules* **2022**, *27* (18), 5847.
(5) Atalar, M. N.; Baran, A.; Baran, M. F.; Keskin, C.; Aktepe, N.; Yavuz, Ö.; İrtegun Kandemir, S. Economic fast synthesis of olive leaf extract and silver nanoparticles and biomedical applications. *Part. Sci. Technol.* **2022**, *40* (5), 589−597.
(6) Amini, S. M. Preparation of antimicrobial metallic nanoparticles with bioactive compounds. *Mater. Sci. Eng., C* **2019**, *103*, 109809.
(7) Nahar, K.; et al. Synthesis and characterization of Silver nanoparticles from Cinnamomum tamala leaf extract and its antibacterial potential. *Int. J. Nano Dimens.* **2020**, *11* (1), 88−98.
(8) Alwhibi, M. S.; Soliman, D. A.; Awad, M. A.; Alangery, A. B.; Al Dehaish, H.; Alwasel, Y. A. Green synthesis of silver nanoparticles: Characterization and its potential biomedical applications. *Green Process. Synth.* **2021**, *10* (1), 412−420.
(9) Ahmed, S. F.; Mofijur, M.; Rafa, N.; Chowdhury, A. T.; Chowdhury, S.; Nahrin, M.; Islam, A. S.; Ong, H. C. Green approaches in synthesising nanomaterials for environmental nanobioremediation: Technological advancements, applications, benefits, and challenges. *Environ. Res.* **2022**, *204*, 111967.
(10) Saratale, G. D.; Saratale, R. G.; Kim, D. S.; Kim, D. Y.; Shin, H. S. Exploiting fruit waste grape pomace for silver nanoparticles synthesis, assessing their antioxidant, antidiabetic potential and antibacterial activity against human pathogens: a novel approach. *Nanomaterials* **2020**, *10* (8), 1457.
(11) Li, J.; Zhang, B.; Chang, X.; Gan, J.; Li, W.; Niu, S.; Kong, L.; Wu, T.; Zhang, T.; Tang, M.; et al. Silver nanoparticles modulate mitochondrial dynamics and biogenesis in HepG2 cells. *Environ. Pollut.* **2020**, *256*, 113430.
(12) Almalah, H. I.; Alzahrani, H. A.; Abdelkader, H. S. Green synthesis of silver nanoparticles using cinnamomum zylinicum and their synergistic effect against multi-drug resistance bacteria. *J. Nanotechnol. Res.* **2019**, *01* (02), 95−107.
(13) Ghumman, S. A.; Bashir, S.; Noreen, S.; Khan, A. M.; Malik, M. Z. Taro-corms mucilage-alginate microspheres for the sustained release of pregabalin: In vitro & in vivo evaluation. *Int. J. Biol. Macromol.* **2019**, *139*, 1191−1202.
(14) Ribeiro Pereira, P.; Bertozzi de Aquino Mattos, É.; Nitzsche Teixeira Fernandes Corrêa, A. C.; Afonso Vericimo, M.; Margaret Flosi Paschoalin, V. Anticancer and Immunomodulatory Benefits of Taro (Colocasia esculenta) Corms, an underexploited tuber crop. *Int. J. Mol. Sci.* **2020**, *22* (1), 265.
(15) Kapcum, C.; Pasada, K.; Kantiwong, P.; Sroysang, B.; Phiwtawee, J.; Suphantharika, M.; Belur, P. D.; Agoo, E. M. G.; Janairo, J. I. B.; Wongsagonsup, R. Effects of different cooking methods on chemical compositions, in vitro starch digestibility and antioxidant activity of taro (Colocasia esculenta) corms. *Int. J. Food Sci. Technol.* **2022**, *57* (8), 5144−5154.
(16) Kamel, R.; Afifi, S. M.; Kassem, I. A.; Elkasabgy, N. A.; Farag, M. A. Arabinoxylan and rhamnogalacturonan mucilage: Outgoing and potential trends of pharmaceutical, environmental, and medicinal merits. *Int. J. Biol. Macromol.* **2020**, *165*, 2550−2564.
(17) Shehata, M. G.; Abd El-Aziz, N. M.; Mehany, T.; Simal-Gandara, J. Taro leaves extract and probiotic lactic acid bacteria: A synergistic approach to improve antioxidant capacity and bioaccessibility in fermented milk beverages. *LWT-Food Sci. Technol.* **2023**, *187*, 115280.
(18) Kumar, V.; Sharma, H. K. Process optimization for extraction of bioactive compounds from taro (Colocasia esculenta), using RSM and ANFIS modeling. *J. Food Meas. Charact.* **2017**, *11*, 704−718.
(19) Baran, M. F.; Keskin, C.; Baran, A.; Hatipoğlu, A.; Yildiztekin, M.; Küçükaydin, S.; Kurt, K.; Hoşgören, H.; Sarker, M. M. R.; Sufianov, A.; et al. Green synthesis of silver nanoparticles from Allium cepa L. Peel extract, their antioxidant, antipathogenic, and anticholinesterase activity. *Molecules* **2023**, *28* (5), 2310.
(20) Amirjani, A.; Firouzi, F.; Haghshenas, D. F. Predicting the size of silver nanoparticles from their optical properties. *Plasmonics* **2020**, *15*, 1077−1082.
(21) Mehta, B. K.; Chhajlani, M.; Shrivastava, B. D. Green synthesis of silver nanoparticles and their characterization by XRD. *J. Phys.: Conf. Ser.* **2017**, *836*, 012050.
(22) Dada, A. O.; Adekola, F. A.; Dada, F. E.; Adelani-Akande, A. T.; Bello, M. O.; Okonkwo, C. R.; Inyinbor, A. A.; Oluyori, A. P.; Olayanju, A.; Ajanaku, K. O.; et al. Silver nanoparticle synthesis by Acalypha wilkesiana extract: phytochemical screening, characterization, influence of operational parameters, and preliminary antibacterial testing. *Heliyon* **2019**, *5* (10), No. e02517.
(23) Gontijo, L. A. P.; Raphael, E.; Ferrari, D. P. S.; Ferrari, J. L.; Lyon, J. P.; Schiavon, M. A. pH effect on the synthesis of different size silver nanoparticles evaluated by DLS and their size-dependent antimicrobial activity. *Matéria (Rio de Janeiro)* **2020**, *25*, 1−10.
(24) Kamshad, M.; Jahanshah Talab, M.; Beigoli, S.; Sharifirad, A.; Chamani, J. Use of spectroscopic and zeta potential techniques to study the interaction between lysozyme and curcumin in the presence of silver nanoparticles at different sizes. *J. Biomol. Struct. Dyn.* **2019**, *37* (8), 2030−2040.
(25) Bhowmik, P.; Modi, B.; Roy, P.; Chowdhury, A. Strategies to combat Gram-negative bacterial resistance to conventional antibacterial drugs: a review. *Osong Public Health and Res. Perspect.* **2023**, *14* (5), 333−346.
(26) Arsène, M. M. J.; Podoprigora, I. V.; Davares, A. K. L.; Razan, M.; Das, M. S.; Senyagin, A. N. Antibacterial activity of grapefruit peel extracts and green-synthesized silver nanoparticles. *Vet. World* **2021**, *14* (5), 1330−1341.
(27) Latham, J.; et al. Enzymatic Cascades. *Applied Biocatalysis: The Chemist's Enzyme Toolbox*; John Wiley & Sons Ltd, 2020, pp 409−474.

https://doi.org/10.1021/acsomega.3c10489
ACS Omega 2024, 9, 12146−12157

(28) Mabrok, H. H. B. Protective role of lignan-converting bacteria on chemically-induced breast cancer in gnotobiotic rats. Ph.D. Thesis, Universität Potsdam, 2013.
(29) Salari, S.; et al. In-vitro evaluation of antioxidant and antibacterial potential of greensynthesized silver nanoparticles using Prosopis farcta fruit extract. *Iran. J. Pharm. Res.* **2019**, *18* (1), 430−455.
(30) Flieger, J.; Franus, W.; Panek, R.; Szymańska-Chargot, M.; Flieger, W.; Flieger, M.; Kołodziej, P. Green synthesis of silver nanoparticles using natural extracts with proven antioxidant activity. *Molecules* **2021**, *26* (16), 4986.
(31) Haseeb, M. T.; Hussain, M. A.; Abbas, K.; Youssif, B. G.; Bashir, S.; Yuk, S. H.; Bukhari, S. N. A. Linseed hydrogel-mediated green synthesis of silver nanoparticles for antimicrobial and wound-dressing applications. *Int. J. Nanomed.* **2017**, *12*, 2845−2855.
(32) Valizadeh, R.; Hemmati, A. A.; Houshmand, G.; Bayat, S.; Bahadoram, M. Wound healing potential of Althaea officinalis flower mucilage in rabbit full thickness wounds. *Asian Pac. J. Trop. Biomed.* **2015**, *5* (11), 937−943.
(33) Mihailović, V.; Srećković, N.; Nedić, Z. P.; Dimitrijević, S.; Matić, M.; Obradović, A.; Selaković, D.; Rosić, G.; Katanić Stanković, J. S. Green synthesis of silver nanoparticles using Salvia verticillata and Filipendula ulmaria extracts: Optimization of synthesis, biological activities, and catalytic properties. *Molecules* **2023**, *28* (2), 808.
(34) Srećković, N. Z.; Nedić, Z. P.; Liberti, D.; Monti, D. M.; Mihailović, N. R.; Katanić Stanković, J. S.; Dimitrijević, S.; Mihailović, V. B. Application potential of biogenically synthesized silver nanoparticles using Lythrum salicaria L. extracts as pharmaceuticals and catalysts for organic pollutant degradation. *RSC Adv.* **2021**, *11* (56), 35585−35599.
(35) Mock, J.; Barbic, M.; Smith, D. R.; Schultz, D. A.; Schultz, S. Shape effects in plasmon resonance of individual colloidal silver nanoparticles. *J. Chem. Phys.* **2002**, *116* (15), 6755−6759.
(36) Vanaja, M.; Gnanajobitha, G.; Paulkumar, K.; Rajeshkumar, S.; Malarkodi, C.; Annadurai, G. Phytosynthesis of silver nanoparticles by Cissus quadrangularis: influence of physicochemical factors. *J. Nanostruct. Chem.* **2013**, *3*, 17.
(37) Pirtarighat, S.; Ghannadnia, M.; Baghshahi, S. Green synthesis of silver nanoparticles using the plant extract of Salvia spinosa grown in vitro and their antibacterial activity assessment. *J. Nanostruct. Chem.* **2019**, *9*, 1−9.
(38) Olajire, A.; Adeyeye, G.; Yusuf, R. Alchornea laxiflora bark extract assisted green synthesis of platinum nanoparticles for oxidative desulphurization of model oil. *J. Cluster Sci.* **2017**, *28*, 1565−1578.
(39) Kotak, D. J.; Devarajan, P. V. Bone targeted delivery of salmon calcitonin hydroxyapatite nanoparticles for sublingual osteoporosis therapy (SLOT). *Nanomedicine* **2020**, *24*, 102153.
(40) Santhoshkumar, J.; VenkatKumar, S. Green synthesis of copper oxide nanoparticles from magnolia champaca floral extract and its antioxidant & toxicity assay using Danio Rerio. *Int. J. Recent Technol. Eng.* **2020**, *8*, 5476−5479.
(41) Ajitha, B.; Ashok Kumar Reddy, Y.; Reddy, P. S. Biogenic nano-scale silver particles by Tephrosia purpurea leaf extract and their inborn antimicrobial activity. *Spectrochim. Acta, Part A* **2014**, *121*, 164−172.
(42) Franzolin, M. R.; Courrol, D. d. S.; Silva, F. R. d. O.; Courrol, L. C. Antimicrobial activity of silver and gold nanoparticles prepared by photoreduction process with leaves and fruit extracts of Plinia cauliflora and Punica granatum. *Molecules* **2022**, *27* (20), 6860.
(43) Banala, R. R.; Nagati, V. B.; Karnati, P. R. Green synthesis and characterization of Carica papaya leaf extract coated silver nano-particles through X-ray diffraction, electron microscopy and evaluation of bactericidal properties. *Saudi J. Biol. Sci.* **2015**, *22* (5), 637−644.
(44) Rautela, A.; Rani, J.; Debnath Das, M. Green synthesis of silver nanoparticles from Tectona grandis seeds extract: characterization and mechanism of antimicrobial action on different microorganisms. *J. Anal. Sci. Technol.* **2019**, *10* (1), 5−10.
(45) Sadeghi, B.; Gholamhoseinpoor, F. A study on the stability and green synthesis of silver nanoparticles using Ziziphora tenuior (Zt) extract at room temperature. *Spectrochim. Acta, Part A* **2015**, *134*, 310−315.
(46) Mahiuddin, M.; Saha, P.; Ochiai, B. Green synthesis and catalytic activity of silver nanoparticles based on Piper chaba stem extracts. *Nanomaterials* **2020**, *10* (9), 1777.
(47) Mortazavi-Derazkola, S.; Yousefinia, A.; Naghizadeh, A.; Lashkari, S.; Hosseinzadeh, M. Green synthesis and characterization of silver nanoparticles using Elaeagnus angustifolia bark extract and study of Its antibacterial effect. *J. Polym. Environ.* **2021**, *29*, 3539−3547.
(48) Singla, S.; Jana, A.; Thakur, R.; Kumari, C.; Goyal, S.; Pradhan, J. Green synthesis of silver nanoparticles using Oxalis griffithii extract and assessing their antimicrobial activity. *OpenNano* **2022**, *7*, 100047.
(49) Lima, D. . d.S.; Gullon, B.; Cardelle-Cobas, A.; Brito, L. M.; Rodrigues, K. A.; Quelemes, P. V.; Ramos-Jesus, J.; Arcanjo, D. D.; Plácido, A.; Batziou, K.; et al. Chitosan-based silver nanoparticles: A study of the antibacterial, antileishmanial and cytotoxic effects. *J. Bioact. Compat. Polym.* **2017**, *32* (4), 397−410.
(50) Bruna, T.; Maldonado-Bravo, F.; Jara, P.; Caro, N. Silver nanoparticles and their antibacterial applications. *Int. J. Mol. Sci.* **2021**, *22* (13), 7202.
(51) Noreen, S.; Hussain, I.; Tariq, M. I.; Iqbal, S.; Batool, F.; Ghumman, S. A.; Noureen, S.; Kausar, T. Influence of Extraction Scheme on the Antioxidant Potential of Caralluma tuberculata. *Not. Sci. Biol.* **2018**, *10* (3), 340−347.
(52) Spiegel, M.; Kapusta, K.; Kołodziejczyk, W.; Saloni, J.; Żbikowska, B.; Hill, G. A.; Sroka, Z. Antioxidant activity of selected phenolic acids−ferric reducing antioxidant power assay and QSAR analysis of the structural features. *Molecules* **2020**, *25* (13), 3088.
(53) Ordonez, A.; Gomez, J.; Vattuone, M.; Lsla, M. Antioxidant activities of Sechium edule (Jacq.) Swartz extracts. *Food Chem.* **2006**, *97* (3), 452−458.
(54) Bedlovičová, Z.; Strapáč, I.; Baláž, M.; Salayová, A. A brief overview on antioxidant activity determination of silver nanoparticles. *Molecules* **2020**, *25* (14), 3191.
(55) Kumar, S.; Pandey, A. K. Chemistry and biological activities of flavonoids: an overview. *Sci. World J.* **2013**, *2013*, 1−16.
(56) Flora, S. J. Structural, chemical and biological aspects of antioxidants for strategies against metal and metalloid exposure. *Oxid. Med. Cell. Longevity* **2009**, *2*, 191−206.

https://doi.org/10.1021/acsomega.3c10489
ACS Omega 2024, 9, 12146−12157